Effects of Inorganic Cation Templates on Octahedral Molecular Sieves of Manganese Oxide

Yan-Fei Shen,[†] Steven L. Suib,*[,†,‡] and Chi-Lin O'Young*[,§]

Contribution from the Department of Chemistry, U-60, University of Connecticut, Storrs, Connecticut 06269-3060, Department of Chemical Engineering and Institute of Materials Science, University of Connecticut, Storrs, Connecticut 06269, and Texaco Research Center, Texaco, Inc., P.O. Box 509, Beacon, New York 12508

Received May 17, 1994[⊗]

Abstract: Five hydrated inorganic divalent cations, Mg^{2+}, Co^{2+}, Ni^{2+}, Cu^{2+}, and Zn^{2+}, have successfully been used as templates for the synthesis of manganese oxide octahedral molecular sieves (OMS-1) having the todorokite structure. The OMS-1 samples have been well characterized by X-ray diffraction, differential scanning calorimetry, thermogravimetric analysis, scanning electron microscopy/energy dispersive X-ray studies, inductively coupled plasma analysis, electron paramagnetic resonance, Fourier transform infrared spectroscopy, thiosulfate titration, and cyclohexane sorption. Catalytic CO oxidation and 2-propanol decomposition were carried out. Results show that these OMS-1 samples with a tunnel size of about 6.9 Å are crystalline and chemically pure. They have the following formulas: $Mg_{3.17}Mn_{5.05}O_{12}\cdot 4.52H_2O$, $Co_{1.84}Mn_{5.59}O_{12}\cdot 3.45H_2O$, $Ni_{1.64}Mn_{5.75}O_{12}\cdot 4.19H_2O$, $Cu_{3.50}Mn_{4.45}O_{12}\cdot 5.33\ H_2O$, and $Zn_{3.55}Mn_{4.47}O_{12}\cdot 2.59H_2O$. Their thermal stability largely depends on the nature of the cations: Mg-OMS-1 is thermally stable in air up to 600 °C; Co-OMS-1 and Ni-OMS-1 are stable to 500 °C, and Cu-OMS-1 and Zn-OMS-1 are stable to 300 °C. The crystal morphologies of the OMS-1 samples can be plates, needles, or fibrous shapes, depending on the nature of the cations. The cations also have profound effects on acidity: Mg-OMS-1, Co-OMS-1, and Ni-OMS-1 have intermediate strength Brønsted and Lewis acid sites, while Cu-OMS-1 and Zn-OMS-1 have no Brønsted acid sites and weak Lewis acid sites. All the OMS-1 samples have six hyperfine electron paramagnetic resonance lines for Mn^{2+} located in an octahedral environment.

Introduction

Octahedral molecular sieves (OMS) are of considerable interest since this new class of molecular sieves may be used in adsorption, catalysis, batteries, and other applications. So far, octahedral molecular sieves including pillared octahedral layered materials have recently been synthesized from the oxides of early transition metals, such as Mo,[1] Ti,[2,3] and Mn.[4-7] These materials have relatively large surface areas and hence are expected to be good catalysts for reactions such as oxidation and oxidative dehydrogenation.

A thermally stable manganese oxide (OMS-1) that has a tunnel size of about 6.9 Å and has a structure of the mineral todorokite has been synthesized in our laboratory[4-6] by the hydrothermal transformation of a manganese oxide layered material similar to the mineral buserite. Hydrated Mg^{2+} cations have been found to act as a template during the transformation and to stabilize the tunnel structure of OMS-1.

Natural todorokite and other minerals found in manganese nodules are found to accommodate some inorganic cations such as Mg^{2+}, Co^{2+}, Ni^{2+}, Cu^{2+}, and Zn^{2+},[8-15] though their cation content differs from one locality to another. Some cations are found to be mobile and capable of stabilizing the structure of the nodules and layered materials.[11,16] Such cations may even be incorporated into the framework of todorokite,[7,9,17] probably by isomorphous substitution for Mn^{2+} cations that exist in the framework of todorokite,[4-6,13] and affect physicochemical properties of todorokite. Cations of Mg^{2+}, Co^{2+}, Ni^{2+}, Cu^{2+}, and Zn^{2+} coordinated with six water molecules have a size similar to the tunnel size of todorokite (ca. 6.9 Å), and they often form isostructural materials such as the spinel, CdI_2, and $Mn(OH)_2$ structures.[19] Therefore, in addition to Mg^{2+} cation, Co^{2+}, Ni^{2+}, Cu^{2+}, and Zn^{2+} cations may be good templates for the transformation of buserite into todorokite and may be isomorphously incorporated into the framework of todorokite.

Natural manganese nodules are found to significantly sorb

* To whom correspondence should be addressed.
† Department of Chemistry, University of Connecticut.
‡ Department of Chemical Engineering and Institute of Materials Science, University of Connecticut.
§ Texaco, Inc.
⊗ Abstract published in *Advance ACS Abstracts*, November 1, 1994.

(1) Lalik, E.; Kolodziejski, W.; Lerf, A; Klinowski, J., *J. Phys. Chem.* **1993**, *97* (1), 223-229.
(2) Watanabe, M.; Fujiki, Y. *J. Solid State Chem.* **1987**, *66*, 56-63.
(3) Anderson, M. W.; Klinowski, J. *Inorg. Chem.* **1990**, *29*, 3260-3263.
(4) Shen, Y.-F.; Zerger, R. P.; Suib, S. L.; McCurdy, L.; Potter, D. I.; O'Young, C.-L. *J. Chem. Soc., Chem. Commun.* **1992**, 1213-1214.
(5) Shen, Y.-F.; Zerger, R. P.; Suib, S. L.; McCurdy, L.; Potter, D. I.; O'Young, C.-L. *Science* **1993**, *260*, 511-515.
(6) DeGuzman, R.; Shen, Y.-F.; Suib, S. L.; Shaw, B. R.; O'Young, C.-L. *Chem. Mater.* **1993**, *5*, 1395-1400.
(7) Golden, G. C.; Chen, C. C.; Dixon, J. B. *Science*, **1986**, *231*, 717-719.
(8) Burns, V. M.; Burns, R. G. *Am. Mineral.* **1978**, *63*, 827-831; *Earth Planet. Sci. Lett.* **1978**, *39*, 341-348.
(9) Burns, V. M.; Burns, R. G. In *Marine Manganese Deposits*; Glasby, G. P., Ed.; Elsevier: New York, 1977; pp 185-248, 461-510.
(10) He, L.-B. *Chin. Sci. Bull.* **1991**, *36*, 1190-1190.
(11) Nimfopoulos, M. K.; Pattrick, R. A. D. *Mineral. Mag.* **1991**, *55*, 423-434.
(12) Kokichi, I.; Sukune, T. *Kozan Chishitsu* **1989**, *39*, 205-207, 325-328.
(13) Rao, P. S.; Pattan, J. N. *Indian J. Mar. Sci.* **1989**, *18*, 11-15.
(14) Siegel, M. D. *Science* 1983, *219*, 172-174.
(15) Larson, T. H. *Am. Mineral.* **1962**, *47*, 59-66.
(16) Giovanoli, R.; Burki, P.; Gioffredi, M.; Stumm, W. *Chimia* **1975**, *29*, 517-520.
(17) Burns, R. G.; Burns, V. M. In *Marine Minerals*; Burns, R. G., Ed.; LithoCrafters: Chelsea, MI, 1979; pp 1-46; *Philos. Trans. R. Soc. London, A* **1977**, *286*, 283-301.
(18) Shen, Y.-F.; Suib, S. L.; O'Young, C.-L. Divalent cation doped todorokite: synthesis, characterization and applications. Manuscript in preparation.
(19) Wells, A. F. *Structural Inorganic Chemistry*; Clarendon Press: Oxford, 1975; pp 210-214, 490-493, 520-522.

0002-7863/94/1516-11020$04.50/0

SO_2,[20-22] H_2S,[20,23] and NH_3[23] as well as catalyze some important reactions, such as the complete oxidation of CO and hydrocarbons,[24,25] selective NO reduction,[26,27] decomposition of organic sulfur compounds,[23] asphalt,[29] and alcohol,[30] demetalation of petroleum residua,[31,32] dehydrogenation of hydrocarbons,[33] etc. These reports indicate potential applications of manganese OMS materials as sorbents for purification of industrial exhaust and waste water, and as catalysts.

The present study focused on finding new templates for the synthesis of new OMS materials and seeing how these templates affect the structures and physicochemical properties of OMS materials.

Experimental Section.

1. Sample Preparation. Manganese oxides with layered structures were prepared in the following way: 50 mL of 5.0 M NaOH was added dropwise into 40 mL of 0.50 M $MnCl_2$ solution (Aldrich) at room temperature under vigorous stirring, to prepare a $Mn(OH)_2$ suspension. The $Mn(OH)_2$ suspension was then added dropwise by 40 mL of 0.10 M $Mg(MnO_4)_2$ (Pfaltz and Bauer) solution at room temperature under vigorous stirring. A black-brown suspension was obtained with a final pH of 13.8. After aging at room temperature for 4 days, the suspension was filtered and washed with distilled deionized water (DDW) until no Cl^- was detected or until the pH was about 7. In this way, a layered material, Na^+-birnessite, was obtained.

Na^+-birnessite suspension was then ion-exchanged with 300 mL of 0.5−1 M aqueous solution of an inorganic salt (Mg^{2+}, Co^{2+}, Ni^{2+}, Cu^{2+}, and Zn^{2+}) at room temperature while stirring overnight. The exchanged product was then filtered and washed with DDW at least 3−5 times to prepare another layered material, buserite. Buserite suspensions were autoclaved at 150−170 °C for about 2 days to prepare todorokite, a tunnel manganese oxide. Todorokite suspensions were filtered and washed with DDW 3−5 times and dried at room temperature in air.

Synthetic todorokite is referred to in this paper as M-OMS-1,[4-6] where M represents the divalent cations in the tunnel of octahedral molecular sieve 1 (OMS-1). For example, Mg-OMS-1 is an OMS-1 material with Mg^{2+} cations in the tunnel.

2. X-ray Diffraction (XRD) Studies. A washed sample suspension was spread on a glass slide and dried in air at room temperature. The dried sample film was calcined in air at different temperatures. XRD patterns were obtained using a Scintag XDS-200 diffractometer with a Cu Kα radiation source. For comparison of peak intensities, the instrument was always operated under the same conditions (incident slits 2 and 4 mm, 45 V, and a current of 40 mA) and all the samples were analyzed within a one-week period.

3. Thermal Analyses. Differential scanning calorimetry (DSC) and thermogravimetric analyses (TGA) were carried out with DuPont DSC 910 and DuPont 951 TGA instruments, respectively. About 4−10 mg of sample powder was loaded into an aluminum sample pan with a cover for DSC and into a platinum sample holder for TGA. Both nitrogen and oxygen gases were used as carrier gases for TGA experiments to check oxygen loss during heating. Only nitrogen was used for DSC. Both oxygen and nitrogen flow rates were about 30 mL/min.

4. Scanning Electron Microscopy (SEM)/Energy Dispersive X-Ray (EDX) Studies. Sample powders were spread uniformly on carbon paste on an aluminum sample holder and then gold coated before SEM photographs were taken in an Amray 1645 scanning electron microscope. For EDX analysis, no gold was coated on the sample. A Philips PV9800 EDAX spectrometer was used with the Super Quant program to analyze relative concentrations.

5. Inductively Coupled Plasma (ICP) Analysis. Solid samples were weighed and dissolved in an HNO_3/H_2O_2 solution, before ICP analyses were performed using a Jarrell Ash 975 instrument. Since SEM/EDX data show no impurities, only manganese and the inorganic cations used for templates were analyzed.

6. Titration by Thiosulfate. Manganese average oxidation states were determined by titration with sodium thiosulfate. A detailed procedure has been described elsewhere.[34]

A 10 mg sample dried at 120 °C overnight was ground to fine powder and put in an Erlenmeyer flask. About 1 mL of NaOH/NaI solution (32 g of NaOH, 60 g of NaI, and 100 mL of DDW) and 2 mL of 1:5 sulfuric acid were added. The flask was shaken for about 10 min to dissolve the powder.

The red-orange solution was titrated with sodium thiosulfate solution (0.1 N solution diluted 20 times) until the color was pale yellow. About 4 mL of starch indicator solution (1 g in 500 mL of boiling water) was added, and more thiosulfate solution was added until the blue color disappeared. Three trials were done for each sample.

7. Cyclohexane Sorption. About 0.2−0.4 g of a powder sample was loaded into a sample cell and evacuated at about 4×10^{-5} torr at different temperatures. After evacuation at each temperature, the cell with the sample was weighed so that the sample weight loss was known. Then, the sample was exposed to cyclohexane vapor at room temperature for about 40 min and weighed again to obtain a total cyclohexane uptake (W_1). Cyclohexane uptake by the cell and the external surface of the sample, designated as W_2, was determined by measuring how much cyclohexane was sorbed by the sample calcined at 700 °C, where the tunnel structure totally collapses. Cyclohexane uptake of the samples reported here was obtained by subtracting W_2 from W_1.

8. Acidity Measurements by Fourier Transform Infrared (FTIR) Experiments. A 10−20 mg self-supported sample wafer was thermally dehydrated at 400 °C under vacuum of ca 5×10^{-5} Torr for 3 h. A blank spectrum was then recorded at room temperature with a Galaxy Model 4020 FT-IR spectrometer, before the wafer was exposed to pyridine vapor at 100 °C for 30 min. Pyridine was purified with a dried 4A zeolite to remove water and with the freeze−pump−thaw technique to eliminate air. Adsorbed pyridine was desorbed at different temperatures under ca. 10^{-5} Torr for 1 h, before IR spectra were recorded at room temperature.

9. Electron Paramagnetic Resonance (EPR) Measurements. Samples were evacuated and sealed in a quartz tube, before EPR spectra were obtained using a Varian E-3 EPR spectrometer at the following operational conditions: 9.05 GHz frequency, 0.5 mW power, room or liquid nitrogen temperature, and a modulation amplitude of about 4 G.

10. Transmission Electron Microscopy (TEM) Measurements. Powdered samples were ground before they were dispersed into either acetone or ethanol and ultrasonically vibrated. Fine particles were then put onto a carbon-coated Cu grid for the TEM measurements. The TEM images and electron diffraction patterns were obtained with a Phillips EM-420 analytical electron microscope (AEM).

Results

1. XRD Analyses. After ion-exchange of Na^+-birnessite with different inorganic cations, XRD patterns were obtained. Only the *d* spacings and relative intensities of the three strongest peaks are listed in Table 1. Mg^{2+}-, Ni^{2+}-, Co^{2+}-, and Cu^{2+}-exchanged layered materials show a strongest peak at 9.6 Å, which is assigned to buserite. Zn^{2+}-, Li^+-, and Mn^{2+}-exchanged layered materials exhibit a much weaker peak at 9.6 Å than Mg^{2+}-,

(20) Zimmerley, S. R. *U.S. Patent* 3330096, 1967.
(21) Van Hecke, M. C.; Bartlett, R. M. *Met. Trans.* **1973**, *4*, 941−947.
(22) Zeitlin, H.; Lee, J. H.; Pong, T. *Atmos. Environ.* **1976**, *10*, 681−682.
(23) Tashiro, Y. Sangyo to Kankyo (in Japanese) **1978**, 90.
(24) (a) Weisz, P. B. U.S. Patent 3214236, 1965. (b) Weisz, P. B. *J. Catal.* **1968**, *10*, 407−408.
(25) Matsuo, K.; Nitta, M.; Aomura, K. *J. Jpn. Pet. Inst.* **1979**, *22*, 212−217.
(26) Wu, S. C.; Chu, C. *Atmos. Environ.* **1972**, *6*, 309−317.
(27) Matsuo, K.; Nitta, M.; Aomura, K. *J. Jpn. Pet. Inst.* **1979**, *22*, 384−387.
(28) Matsuo, K.; Nitta, M.; Aomura, K. *J. Jpn. Pet. Inst.* **1976**, *19*, 290−294.
(29) Matsuo, K.; Nitta, M.; Aomura, K. *J. Jpn. Pet. Inst.* **1975**, *18*, 697−698.
(30) Matsuo, K.; Nitta, M.; Aomura, K. *J. Jpn. Pet. Inst.* **1976**, *19*, 745−749.
(31) Chang, C. D.; Silvestri, A. J. *Ind. Eng. Chem. Process. Des. Dev.* **1974**, *13*, 315−316.
(32) Fischer, R. H.; Garwood, W. E.; Heineman, H. *Ind. Eng. Chem. Process. Des. Dev.* **1976**, *15*, 570−573.
(33) Nitta, M.; Matsuo, K.; Aomura, K. *Chem. Lett.* **1979**, 125−127.
(34) Murray, J. W.; Balistieri, L. S.; Paul, B. *Geochim. Cosmochim. Acta* **1984**, *48*, 1237−1242.

Table 1. Effective Ionic Radii of Template Cations and XRD Data of Corresponding Exchanged Layered Materials

ion	coordination number	size[a] (Å)	relative XRD peak intensity 9.6 Å	7.1 Å	4.8 Å
Al^{3+}	6	0.68	0	100	0
Ba^{2+}	6	1.49	0	100	0
Co^{2+}	6	0.88	100	0	55
Cu^{2+}	6	0.87	100	30	55
Hg^{2+}	2	0.83	0	100	0
	6	1.16			
K^{+}	6	1.52	0	100	0
Li^{+}	6	0.90	35	100	15
Mg^{2+}	6	0.86	100	0	55
Mn^{2+}	6	0.81	30	100	18
Ni^{2+}	6	0.83	100	0	55
Rb^{+}	6	1.66	0	100	0
Ti^{3+}	6	0.81	0	100	0
Zn^{2+}	6	0.88	35	5	100

[a] From Shannon, R. D. *Acta Crystallogr.* **1976**, *A32*, 7510.

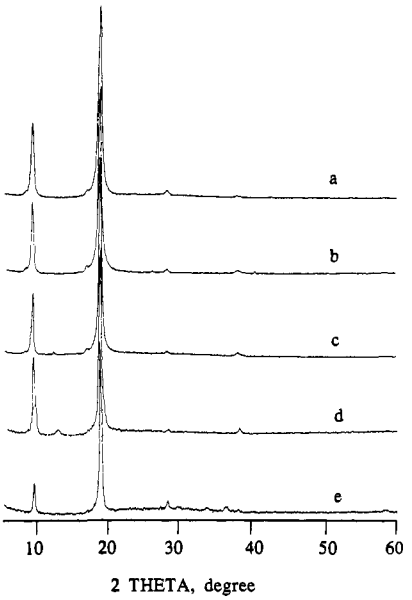

Figure 1. XRD patterns of OMS-1 samples: (a) Mg-OMS-1; (b) Co-OMS-1; (c) Ni-OMS-1; (d) Cu-OMS-1; (e) Zn-OMS-1.

Ni^{2+}-, Co^{2+}-, and Cu^{2+}-exchanged layered materials. When the other cations listed in Table 1 are exchanged into Na^{+}-birnessite, no XRD peak at 9.5−9.6 Å is found. The peak at 7.1 Å due to Na^{+}-birnessite is retained, but peak intensity and sharpness vary from one sample to another. For alkali-metal or some alkaline-earth-metal (e.g., Ba^{2+}) cation-exchanged samples, the peak at 7.1 Å is strong and sharp. For other samples, the peak is weak and broad, indicating that the crystallinity of layered materials or the ordering of the cations in the interlayer is poor, due to the ion-exchange process.

Figure 1 shows the XRD patterns of five autoclaved buserite samples, designated Mg-OMS-1 (Figure 1a), Ni-OMS-1 (Figure 1b), Co-OMS-1 (Figure 1c), Cu-OMS-1 (Figure 1d), and Zn-OMS-1 (Figure 1e). All these five samples show two XRD peaks at 9.5−9.6 and 4.8 Å that are believed to be two of the diagnostic lines for todorokite.[8] Cu-OMS-1 has an additional peak at about 7.1 Å. As can be seen, the five OMS-1 samples are quite crystalline and do not show phases due to other manganese oxides.

The shoulders on the OMS-1 reflections in Figure 1 may be due to unconverted buserites in some of these materials. The 7.1 Å peak for Ni-OMS-1 may be due to Mn-buserite, but a clear assignment is not apparent. The Co-OMS-1 material has additional reflections not observed with the other M-OMS-1 materials. In the case of Zn-OMS-1, manganese oxide impurities are clearly present. These may be associated with the difficulty of incorporating Zn^{2+} into octahedral sites. This may in turn relate to the low degree of thermal stability and acidity of Zn-OMS-1 (vide infra).

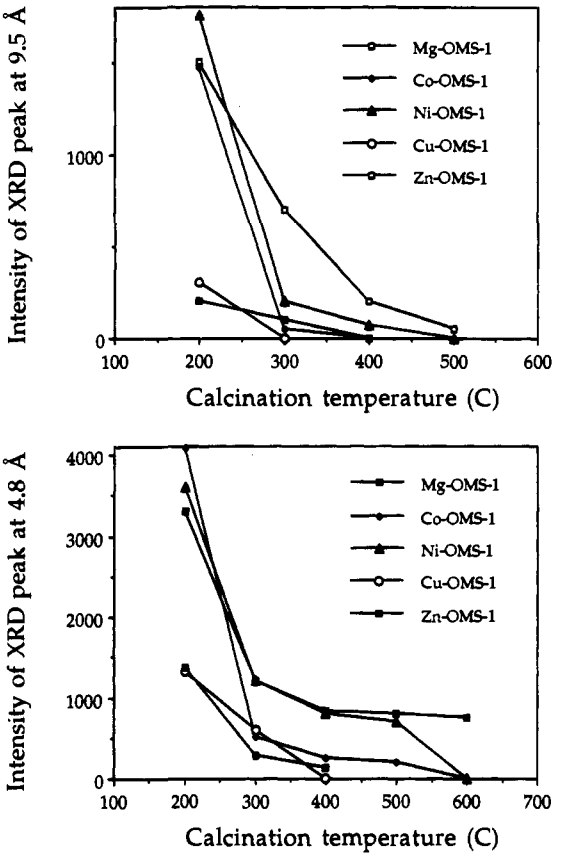

Figure 2. Intensity of the XRD peak of OMS-1 samples as a function of calcination temperature: (top) XRD peak at 9.5 Å; (bottom) XRD peak at 4.8 Å.

XRD patterns were recorded for the autoclaved samples calcined at different temperatures. The intensities of the peaks at 9.5−9.6 and 4.8 Å are plotted against calcination temperature, as shown in Figures 2 (top and bottom, respectively). At 200 °C, all samples show the two peaks at about 9.5 and 4.8 Å with different peak intensities. At 300 °C, Mg-OMS-1 and Ni-OMS-1 still have rather strong peaks at 9.5 and 4.8 Å. Co-OMS-1 and Zn-OMS-1 show weak peaks at 9.5 Å and rather strong peaks at 4.8 Å, and Cu-OMS-1 shows no peak at 9.5 Å and a weak peak at 4.8 Å. Zn-OMS-1 calcined at 300 °C also has new peaks at 2.47, 3.06, and 2.72 Å (Figure 3a), which are assigned to the $ZnMn_2O_4$ phase. At 400 °C, a weak peak at 9.5 Å and a quite strong peak at 4.8 Å are still retained for Mg-OMS-1 and Ni-OMS-1. Only the peak at 4.8 Å is retained for Co-OMS-1 and Zn-OMS-1. Cu-OMS-1 starts forming a $CuMn_2O_4$ phase at 400 °C, which has peaks at 2.52, 2.96, and 1.60 Å (Figure 3b). At 500 °C, only Mg-OMS-1 has both peaks at 9.5 and 4.8 Å, and Co-OMS-1 and Ni-OMS-1 still have peaks at 4.8 Å and no new peaks. At 600 °C, Mg-OMS-1 still has a peak at 4.8 Å and no peak at 9.5 Å (Figure 3c). Co-OMS-1 and Ni-OMS-1 calcined at 600 °C give new crystalline phases (Figure 3d,e), which cannot be assigned to known compounds. At 700 °C, Mg-OMS-1 (Figure 3f), Co-OMS-1 (Figure 3g) and Ni-OMS-1 (Figure 3h) are converted to spinel-type compounds, such as $MgMn_2O_4$, (Co, Mn)(Co, $Mn)_2O_4$, and $NiMn_2O_4$.

A reviewer has suggested that there may be anion effects and cation effects during the exchange step in the preparation of buserite. Our data clearly show a significant cation effect on the crystallization kinetics of OMS-1 or todorokite phases.

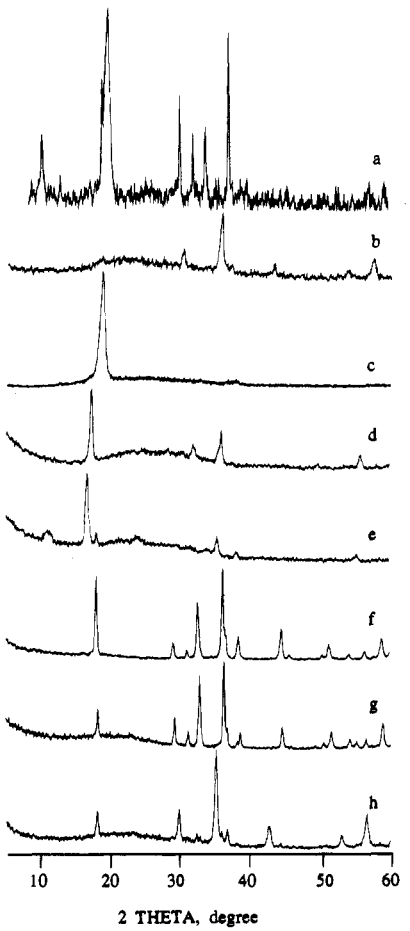

Figure 3. XRD patterns of calcined OMS-1 samples: (a) Zn-OMS-1 calcined at 300 °C; (b) Cu-OMS-1 calcined at 400 °C; (c) Mg-OMS-1 calcined at 600 °C; (d) Co-OMS-1 calcined at 600 °C; (e) Ni-OMS-1 calcined at 600 °C and (f) Mg-OMS-1 calcined at 700 °C; (g) Co-OMS-1 calcined at 700 °C; (h) Ni-OMS-1 calcined at 700 °C.

For example, $Mg(MnO_4)_2$ reagents produce much more crystalline OMS materials than other MnO_4^- reagents.

In summary, inorganic cations have profound effects not only on the nature of the resulting layered and tunnel materials but also on the purity, crystallinity, and thermal stability of the final OMS-1 samples.

2. Thermal Analyses. DSC profiles of the five OMS-1 samples are given in Figure 4. The samples exhibit different thermal behavior. Co-OMS-1 shows two large endotherms at 200 and 320 °C and a small endotherm at 500 °C. Ni-OMS-1 shows a large and broad endotherm around 280 °C and three small endotherms at 350, 450, and 500 °C. Cu-OMS-1 has three endotherms: a small peak at 230 °C and two large peaks at 320 and 490 °C. Zn-OMS-1 shows a strong and sharp endotherm at about 360 °C and a small endotherm at 470 °C. Mg-OMS-1 only shows two endotherms at about 220−230 and 355 °C; no other peaks can be found at temperatures <550 °C.

For Mg-OMS-1, Co-OMS-1, and Ni-OMS-1, the endothermic transitions below 400 °C may be mainly due to water evolution.[35] TGA data (vide infra) also show small amounts of oxygen being removed from Co-OMS-1 and Ni-OMS-1 below 400 °C. For Cu-OMS-1 and Zn-OMS-1, however, the endotherms below 400 °C cannot be attributed only to water evolution, since there is no XRD peak around 9.5 Å. A $ZnMn_2O_4$ phase forms when these two samples are calcined at 300 °C (Figure 2). Lattice oxygen and water may contribute to the endotherms below 400 °C for Cu-OMS-1 and Zn-OMS-1.

(35) Bish, D. L.; Post, J. E. *Am. Mineral.* **1989**, *74*, 177−180.

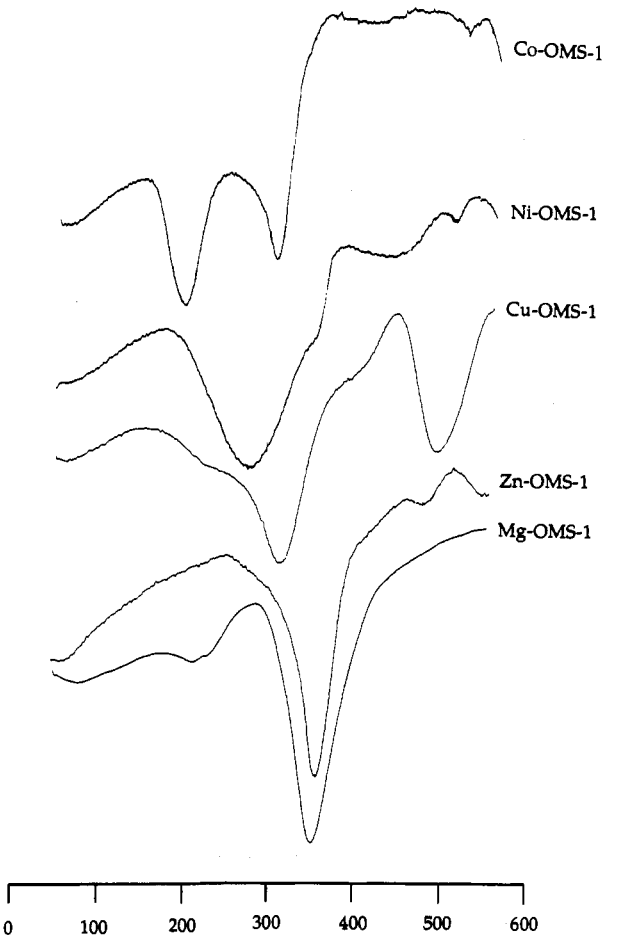

Figure 4. DSC profiles of OMS-1 samples.

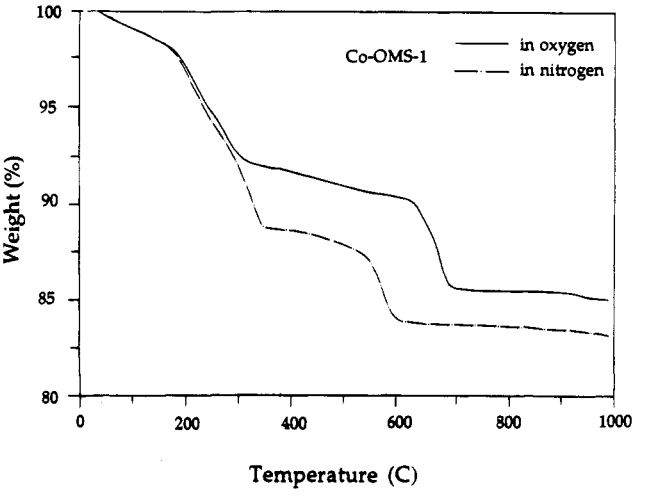

Figure 5. TGA profiles of Co-OMS-1.

TGA profiles (Figures 5−9) are also significantly different for different samples. For example, Co-OMS-1 (Figure 5) has three major weight losses. The first weight loss (40−160 °C) might be due to water physically sorbed on the surface. The second weight loss (180−300 °C) can be mostly attributed to water bound in the tunnel. Oxygen starts being evolved at 300 °C. The amount of oxygen evolved is about 3 wt %, which is calculated from the difference of the nitrogen and oxygen curves in the region of 350−500 °C. In a nitrogen stream, a phase transition occurs at about 540 °C, which can be assigned to a transformation of Co-OMS-1 to an unknown crystalline phase (Figure 3d). This phase transition is delayed to about 630 °C

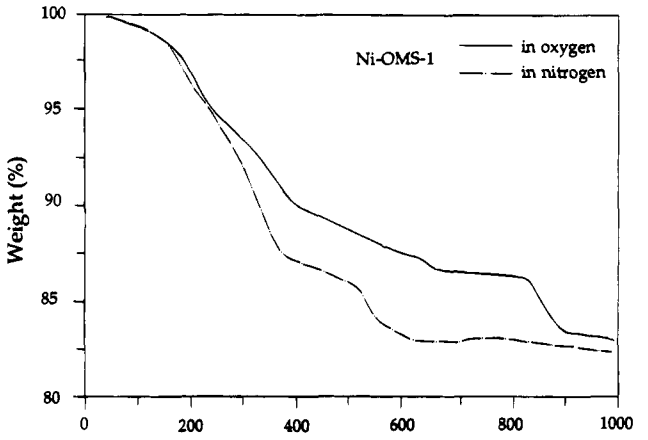

Figure 6. TGA profiles of Ni-OMS-1.

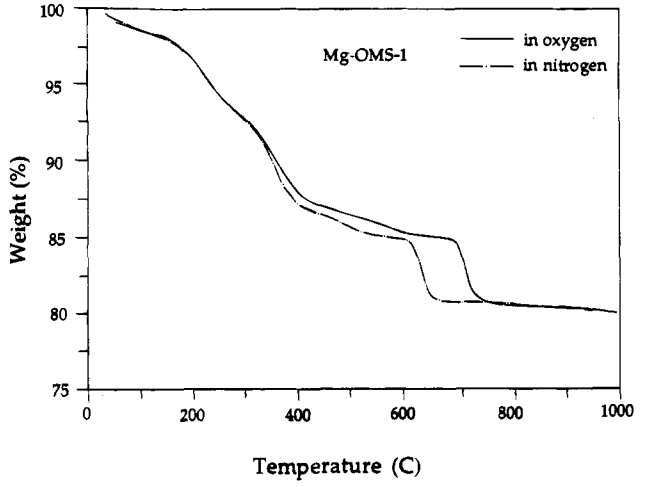

Figure 7. TGA profiles of Mg-OMS-1.

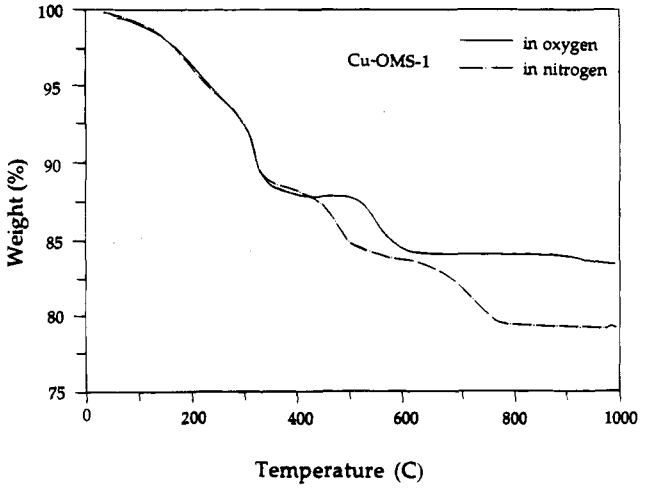

Figure 8. TGA profiles of Cu-OMS-1.

in an oxygen stream. The nitrogen curve still has about 1.8% larger weight loss than the oxygen curve when the temperature is further increased, indicating a gradual oxygen loss at high temperatures.

In the case of Ni-OMS-1 (Figure 6), two major weight losses are found in the regions of 180−350 and 510−550 °C when nitrogen is used as a carrier gas, while three weight losses are observed in the regions of 180−350, 640−650, and 830−890 °C when oxygen is used as a carrier gas. The oxygen loss is about 2.5 wt % in the region of 350−500 °C. The loss around 180−350 °C may be mainly due to water evolution, since the temperature range for this weight loss is the same for both carrier gases and because the todorokite structure is still retained below

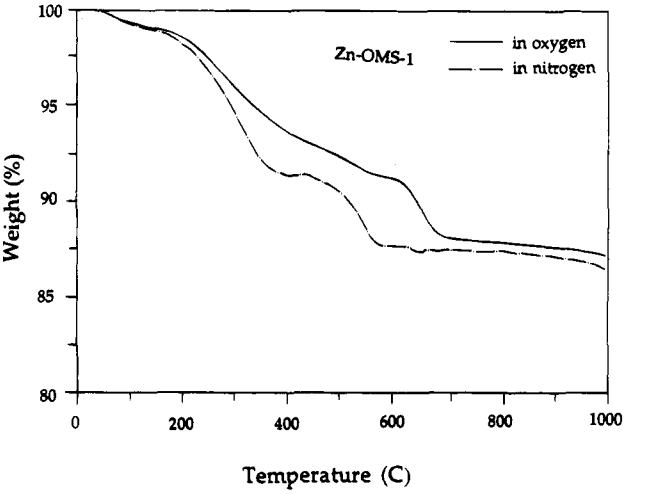

Figure 9. TGA profiles of Zn-OMS-1.

500 °C (Figures 2 and 15c). The weight loss around 510−550 °C in nitrogen and around 640−650 °C in oxygen may be ascribed to a phase transition of todorokite to $NiMn_2O_4$ or a similar compound (Figure 3). The loss around 830−890 °C in oxygen is probably due to the transition of Mn_2O_3 to Mn_3O_4.[8]

Mg-OMS-1 (Figure 7) shows a very small oxygen evolution at temperatures from 180 °C to 550 °C in contrast to the above samples, since the nitrogen and oxygen curves almost overlap. A structural transition of todorokite to $MgMn_2O_4$ (Figure 3) is delayed from 610 °C in nitrogen to 690 °C in oxygen. The difficulty in removing oxygen might be related to the high thermal stability of Mg-OMS-1 (Figures 2 and 3d).

Cu-OMS-1 (Figure 8) has no considerable oxygen evolution until about 420 °C, since the oxygen and nitrogen curves almost overlap below 420 °C. In nitrogen, two phase transitions occur around 420−480 °C and 620−750 °C, while in oxygen only one transition is observed around 510−590 °C. Oxygen evolution takes place at temperatures above 420 °C, especially 700 °C.

In the case of Zn-OMS-1 (Figure 9), oxygen starts being evolved at about 180 °C. The amount is about 1.5 wt % in the temperature region of 300−480 °C. There is only one clear phase transition around 500 °C in nitrogen and around 600 °C in oxygen. At temperatures above 660 °C, only a small amount of oxygen is constantly evolved.

In summary, inorganic cations have strong effects on the thermal behavior of the OMS-1 samples. Water content in the tunnel is also affected by the type of cation. The weight losses in streams of oxygen at 400 °C are as follows: 12.5% for Mg-OMS-1, 8% for Co-OMS-1, 10% for Ni-OMS-1, 12% for Cu-OMS-1, and 6% for Zn-OMS-1. Water coordination appears to be different for different samples, since DSC and TGA curves at temperatures from 300 to 400 °C are different. Oxygen evolution is also affected. Oxygen evolution at temperatures below 400 °C decreases as follows: Co-OMS-1 (3 wt %) > Ni-OMS-1 (2.5 wt %) > Zn-OMS-1 (1.5 wt %) > Mg-OMS-1 (0 wt %) = Cu-OMS-1 (0 wt %). Thermal stability decreases as follows: Mg-OMS-1 > Ni-OMS-1 > Co-OMS-1 > Cu-OMS-1 = Zn-OMS-1. The same sequence is found for the formation of spinel compounds. All these effects may be related to the tendency of these specific transition-metal cations to prefer an octahedral geometry, to Mn−O bond strengths, to cation distributions and locations in tunnels or in the framework, to interaction of the cations with oxygen, manganese, and water, etc.

3. Elemental Analyses. Table 2 shows SEM/EDX data for the OMS-1 samples. Only Mn and M^{2+} contents are detected, indicating that the OMS-1 samples are chemically pure. Since

Table 2. SEM/EDX Data of OMS-1 Samples

	relative elemental composition (wt %)					
sample	Mg	Co	Ni	Cu	Zn	Mn
Mg-OMS-1	1.01					98.99
Co-OMS-1		15.71				84.29
Ni-OMS-1			7.99			92.01
Cu-OMS-1				36.00		74.00
Zn-OMS-1					43.59	56.41

Table 3. Elemental Compositions of the OMS-1 Samples Analyzed by ICP and Average Manganese Oxidation States Determined by Thiosulfate Titrations

	elemental composition (wt %)						av Mn
sample	Mg	Co	Ni	Cu	Zn	Mn	valency
Mg-OMS-1	11.8					42.5	3.50
Co-OMS-1		13.9				39.4	3.64
Ni-OMS-1			12.8			41.9	3.60
Cu-OMS-1				27/8		30.6	3.82
Zn-OMS-1					29.8	31.5	3.78

the instrument does not provide quantitative data for light elements, oxygen and hydrogen are not analyzed and hence only relative percentages of Mn and M^{2+} are presented in Table 3. The following sequence is obtained for cation weight percents: Zn > Cu > Co > Ni > Mg. A sequence for Mn weight percent is as follows: Mg-OMS-1 > Ni-OMS-1 > Co-OMS-1 > Cu-OMS-1 > Zn-OMS-1.

To determine absolute compositions, ICP analyses were done. Results are presented in Table 3. ICP data give the following sequence for cation atomic percentage: Mg > Zn > Cu > Co > Ni. Another sequence is found for Mn atomic percentage: Mg-OMS-1 > Ni-OMS-1 > Co-OMS-1 > Zn-OMS-1 > Cu-OMS-1.

Table 3 also shows the average oxidation states of manganese determined by thiosulfate titrations. The average oxidation states range from 3.5 to 3.8 depending on the nature of the divalent cation. The following sequence of the average oxidation states is found: Mg-OMS-1 < Co-OMS-1 = Ni-OMS-1 < Cu-OMS-1 = Zn-OMS-1. This sequence is quite similar to the sequence for thermal stability of the OMS-1 samples, as described above.

4. EPR Measurements. Pure OMS-1 and layered materials show extremely broad EPR signals. All the samples show six hyperfine Mn^{2+} signals with a g value of 1.98, as is the case for Mn^{2+}-doped molecular sieves.[36] A hyperfine splitting of 99 G indicates that Mn^{2+} cations are present in an octahedral environment. Six hyperfine signals are clearly observed for Mn^{2+} in Cu-OMS-1. At room temperature, Cu-OMS-1 also shows a Cu^{2+} EPR signal with a g value of 2.19, which has been assigned to $[Cu(H_2O)_6]^{2+}$.[37] At 77 K, there are additional peaks between the hyperfine signals. These additional EPR peaks have been attributed to $Dm_I = \pm 1$ and ± 2 forbidden transitions.[38-39] In addition, there is a Cu^{2+} peak with a g value of 2.08 that has been observed in Cu^{2+}-exchanged clay and assigned to "immobile" Cu^{2+} species.[37]

5. Acidity Measurements. IR transmission spectra of pyridine adsorption are shown in Figures 10–13. When desorption is performed at 100 °C, Mg-OMS-1 (Figure10) shows a sharp peak at 1444 cm^{-1}, which is assigned to pyridine adsorbed on Lewis acid sites, and a peak at 1550 cm^{-1} due to pyridine adsorbed on Brønsted acid sites. When the desorption temperature is increased to 200 °C, the intensities of both peaks are considerably decreased. For desorption at 300 °C, all peaks disappear. These results indicate the existence of both Brønsted and Lewis acid sites on Mg-OMS-1. In addition, the broadness of three peaks between 1600 and 1550 cm^{-1} appears to indicate the presence of more than one type of Brønsted acid site.

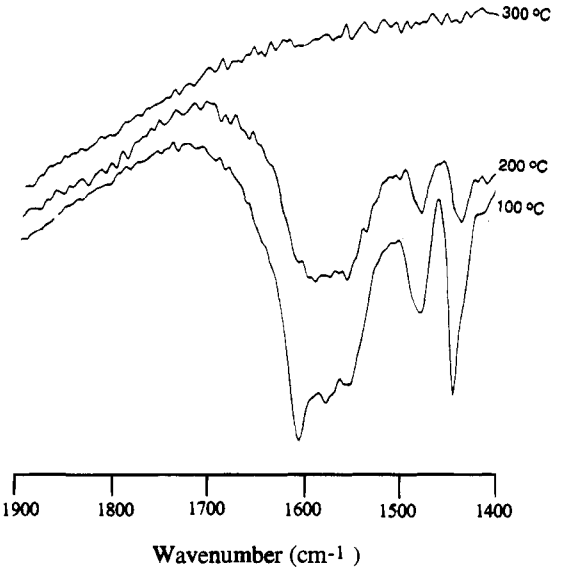

Figure 10. IR spectra of pyridine adsorbed on Mg-OMS-1 and desorbed at different temperatures.

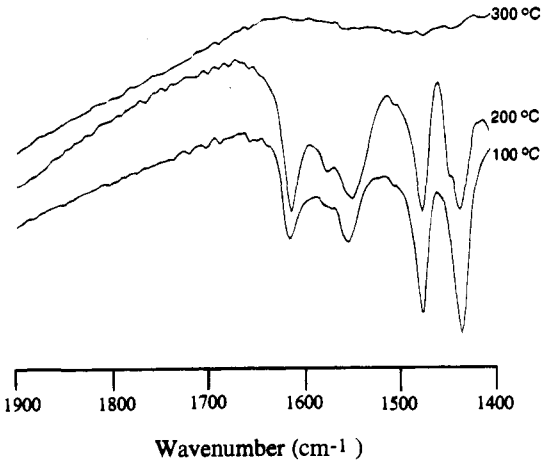

Figure 11. IR spectra of pyridine adsorbed on Co-OMS-1 and desorbed at different temperatures.

In the case of Co-OMS-1 (Figure 11), peaks at 1437 and 1550 cm^{-1} are still intense and well-defined when desorption is performed at 100 and 200 °C. Like Mg-OMS-1, all the peaks disappear upon desorption at 300 °C. These results appear to show that the acidity of Co-OMS-1 is slightly stronger than that of Mg-OMS-1.

Ni-OMS-1 (Figure 12) also has intense peaks at 1433 and 1548 cm^{-1} when desorption is carried out at 100 and 200 °C. An additional peak at 1622 cm^{-1} is found, which is probably also due to pyridine adsorbed on Brønsted acid sites. When desorption is done at 300 °C, weak peaks at 1433 and 1548 cm^{-1} are still observed. These results indicate that Ni-OMS-1 has stronger Brønsted and Lewis acidity than Mg-OMS-1 and Co-OMS-1.

Figure 13 shows IR spectra for Cu-OMS-1 (Figure 13a) and Zn-OMS-1 (Figure 13b). Cu-OMS-1 has very weak Lewis acidity and has no Brønsted acidity, even when desorption is

(36) Brouet, G.; Chen, X. H; Lee, C. W.; Kevan, L. *J. Am. Chem. Soc.* **1992**, *114* (10), 3720–3726.
(37) Barklie, R. C.; Braddell, O.; Doff, D. H. In *Pillared Layered Structures Current Trends and Applications*; Mitchell, I. V. Ed.; Elsvier Applied Science: New York, 1990; pp 219–224.
(38) Rubio O. J.; Munoz P. E.; Boldu O. J.; Chen, Y.; Abraham, M. M. *J. Chem. Phys.* 1979, *72* (2), 633–638.
(39) De Wijn, H. W.; Van Balderen, R. F. *J. Chem. Phys.* **1967**, *46*(4), 1381–1388.

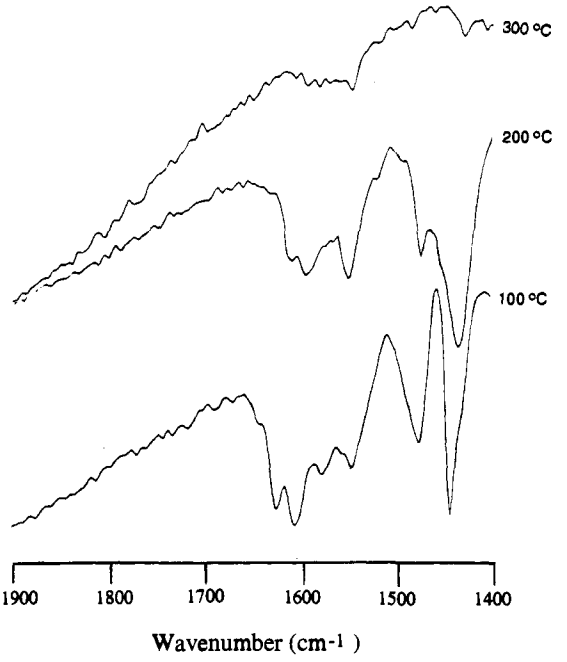

Figure 12. IR spectra of pyridine adsorbed on Ni-OMS-1 and desorbed at different temperatures.

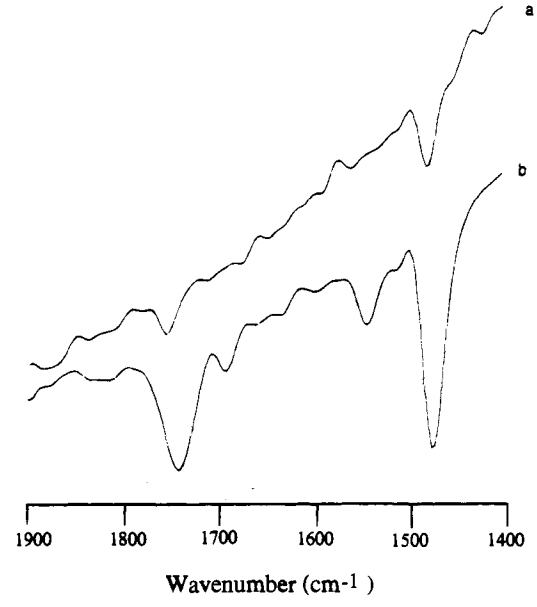

Figure 13. IR spectra of pyridine adsorbed on (a) Cu-OMS-1 and (b) Zn-OMS-1 desorbed at 100 °C.

performed at 100 °C. Zn-OMS-1 has rather strong Lewis acid sites and some Brønsted acid sites.

In summary, Mg-OMS-1, Co-OMS-1, Zn-OMS-1, and Ni-OMS-1 samples have intermediate strength Lewis and Brønsted acid sites, while Cu-OMS-1 has weak Lewis acid sites and no Brønsted acid sites. The following sequence of decreasing overall acidity is found: Ni-OMS-1 > Co-OMS-1 > Mg-OMS-1 > Zn-OMS-1 > Cu-OMS-1.

6. SEM Studies. SEM micrographs are shown in Figure 14. Mg-OMS-1 has a platelike shape with a size of about 0.5−3 mm (Figure 14a). The plates are irregular in shape and can aggregate to form large particles; Co-OMS-1 clearly contains both needle- and plate-shaped crystallites (Figure 14b). Needles are well shaped with lengths of about 4−5 mm, and the cross sections of the needles appear to be rectangular or square with sizes of about 0.2−0.3 mm. The shapes of the plates of Co-OMS-1 crystallites are also irregular. The other three samples, Ni-OMS-1 (Figure 14c), Cu-OMS-1 (Figure 14d), and Zn-OMS-1 (Figure 14e), mostly consist of plate-shaped crystallites, as is the case for Mg-OMS-1. These results show that crystallites of the OMS-1 samples have three kinds of shapes: plates, needles, and fibers, depending on the nature of the cations.

7. Uptake of Cyclohexane. Uptakes of cyclohexane and weight losses of the OMS-1 samples are plotted against dehydration temperature, as shown in Figure 15. The uptake curves are considerably different for different samples. Uptake of cyclohexane by Mg-OMS-1 (Figure 15a) increases with dehydration temperature up to 500 °C and then significantly decreases. Cyclohexane uptake for Co-OMS-1 (Figure 15b) and Ni-OMS-1 (Figure 15c) samples increases with temperature up to 400 °C and drops very slightly at 500 °C and significantly at 600 °C. Uptakes of cyclohexane for Cu-OMS-1 (Figure 15d) increase with temperature up to 200 °C. The uptake decreases slightly at 300 °C and considerably at higher temperatures. Zn-OMS-1 (Figure 15e) sorbs cyclohexane increasingly with temperature to about 100 °C. The uptake then decreases slowly with temperature up to 300 °C and substantially with a further increase in temperature. The maximum uptake also varies from one sample to another. The order of maximum uptake is as follows: Zn-OMS-1 (19.1 g/100 g) > Ni-OMS-1 (18.6 g/100 g) > Mg-OMS-1 (18.2 g/100 g) > Cu-OMS-1 (16.2 g/100 g) > Co-OMS-1 (10.4 g/100 g). These uptake results are consistent with the presence of the tunnel size of todorokite (6.9 Å) and the thermal stability of the materials.

A reviewer has suggested that since the molecular weights of the five cation forms of OMS-1 reported here are different, that a grams of cyclohexane to 100 g of OMS-1 comparison is problematic. If corrections for molecular weight are taken into account, the order of maximum uptake is Mg > Ni > Zn > Cu > Co. This ordering, except for the Co-OMS-1 sample, is closely related to the order of thermal stability and degree of crystallinity.

Discussion

1. Tunnel Structure. All the above-mentioned OMS-1 samples show two XRD peaks at 9.6 and 4.8 Å, which are believed to be diagnostic lines for todorokite.[8] Mg^{2+}-, Co^{2+}-, Ni^{2+}-, Cu^{2+}-, and Zn^{2+}-exchanged layered materials, which are precursors for the synthesis of corresponding todorokite samples, also show these two peaks at 9.6 and 4.8 Å, though their relative peak intensities are different (Table 1 and Figure 1). This similarity in XRD peak positions of the two materials indicates that XRD results alone should not be used as diagnostic evidence for the presence of todorokite. Comprehensive structural, thermal, and surface analyses should be done.

One factor of considerable importance is the difference in thermal stability of the layered materials and todorokite. It is found that calcining the above-mentioned precursor layered materials at 100 °C shifts the peak at 9.6 Å to 7.1 Å; that is, a water layer in the interlayer appears to be removed during calcination. Todorokite, however, retains the peak at 9.6 Å when calcined at temperatures as high as 500 °C (Figure 2), depending on the nature of the cations.

Other evidence for the presence of the todorokite structure in these transition-metal template systems comes from cyclohexane uptake results (Figure 15). Cyclohexane has a size of about 0.47 × 6.2 × 0.69 Å and is only significantly sorbed by large-pore zeolites like ZSM-12, mordenite, and Y-zeolite.[40] Cyclohexane uptake is related to the minimum size of the todorokite tunnel and stability of the tunnel structure. Figure 15 shows that all the OMS-1 samples can sorb significant

(40) Wilson, S. T.; Lok, B. M.; Messina, C. A.; Cannan, T. R.; Flanigen, E. M. Intrazeolite Chemistry ACS Symp. Ser. **1983**, *218*, 79−82.

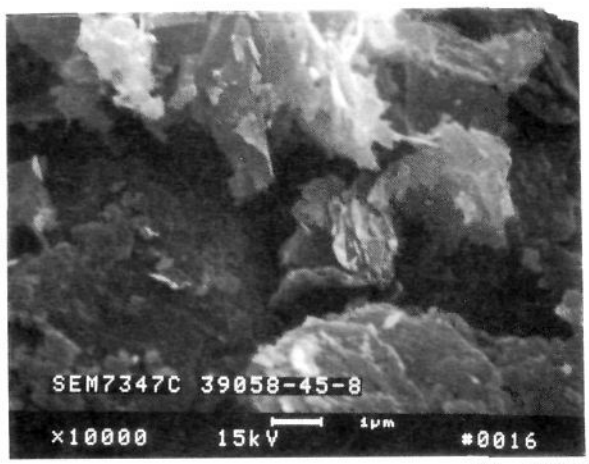

Mg-OMS-1

Co-OMS-1

Ni-OMS-1

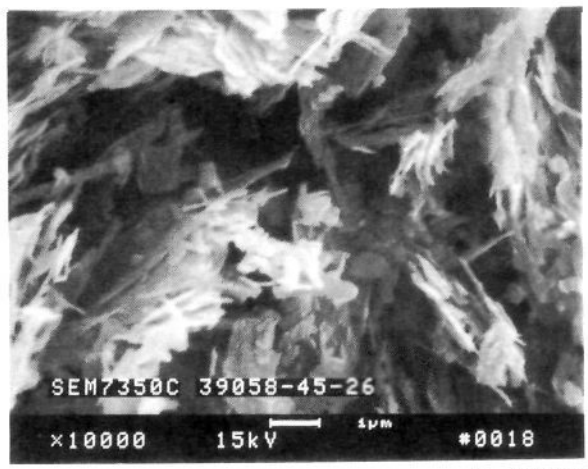

Cu-OMS-1

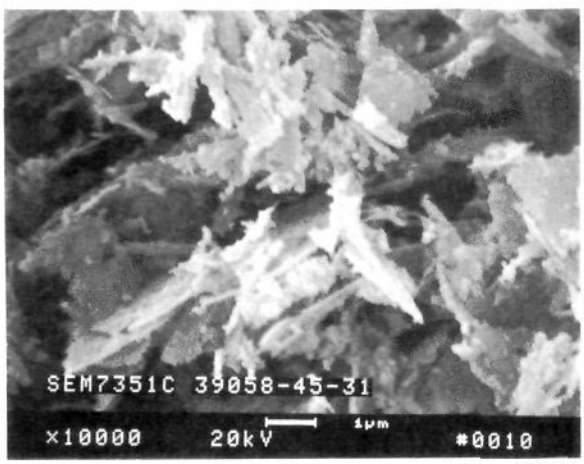

Zn-OMS-1

Figure 14. SEM photographs of (a, top left) Mg-OMS-1, (b, top right) Co-OMS-1, (c, middle left) Ni-OMS-1, (d, middle right) Cu-OMS-1, and (e, bottom) Zn-OMS-1.

amounts of cyclohexane (similar to or greater than large-pore zeolites[40] or pillared clays[41]), although the maximum uptake and thermal dependence of the uptake are different for different OMS-1 samples.

Nitta reports[42] that various manganese nodules also have tremendous sorption capacity in a range similar to that of the OMS materials reported here. Uptake for OMS-1 samples increases with dehydration temperature, indicating removal of tunnel water and an increase of void volume for cyclohexane accommodation. A decrease in uptake with increasing temperature indicates partial or total collapse of the tunnel structure. Therefore, the temperature dependence of the uptake is related to the thermal stability of the OMS-1 sample, which in turn is related to the interaction of the cations with the framework of todorokite.

The structural ramifications of the uptake data discussed

(41) Kikuchi, E.; Matsuda, T. *Catal. Today*, **1988**, *2*, 297–302.
(42) Nitta, M. *Appl. Catal.* **1984**, *9*, 151–176.

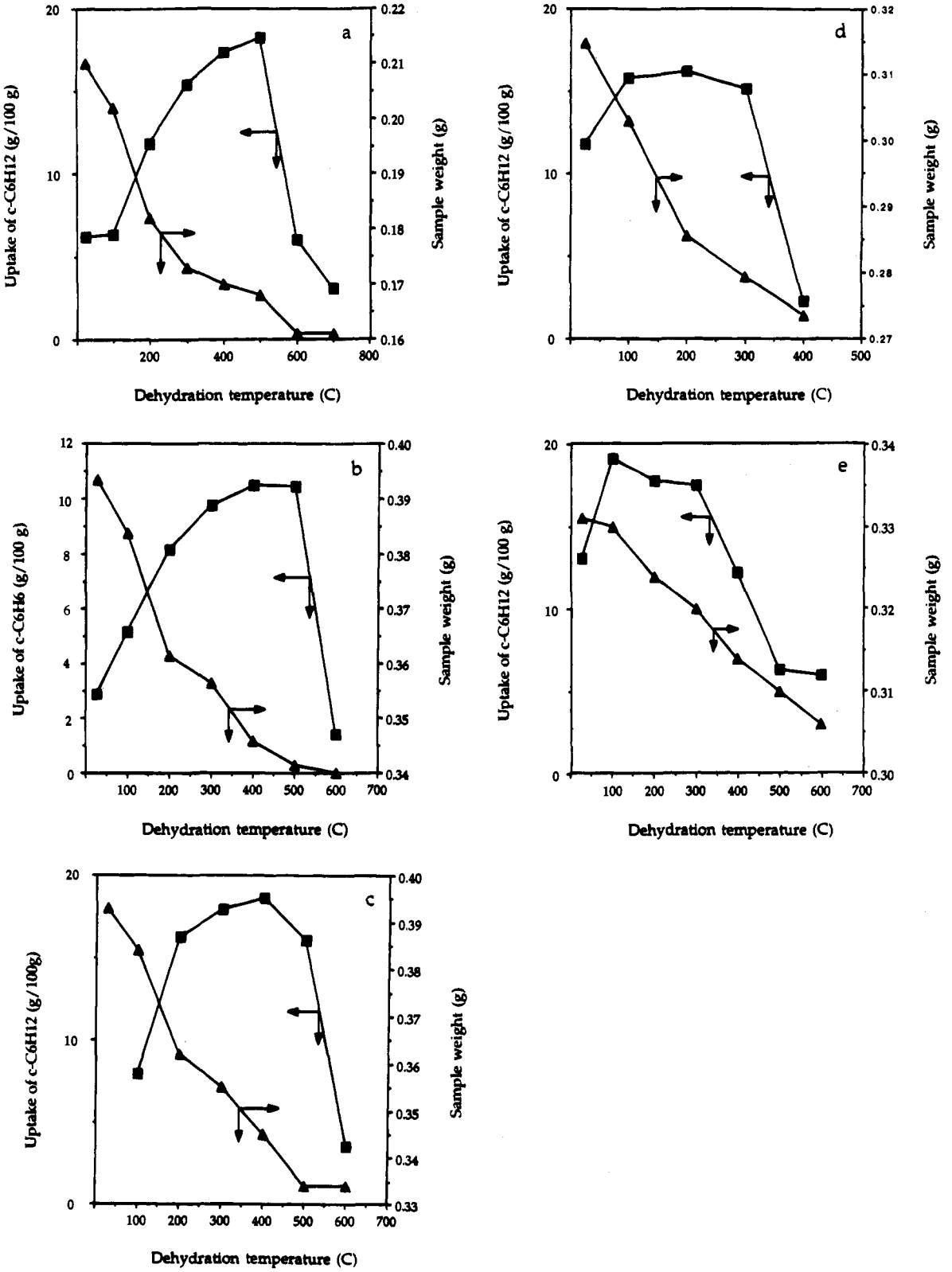

Figure 15. Cyclohexane uptake and weight loss as a function of dehydration temperature: (a) Mg-OMS-1; (b) Co-OMS-1; (c) Ni-OMS-1; (d) Cu-OMS- 1; (e) Zn-OMS-1.

above are further confirmed by transmission electron microscopy (TEM) and electron diffraction results. The presence of different size tunnel cations leads to a change in the *b* and *c* lattice parameters. These data suggest that the transition-metal cations in the tunnels act as templates and allow the tunnels to expand or contract depending on the size of the cation. This behavior helps explain the vast differences in cation content and structural parameters for manganese nodules.[8,9,11,15,17,24,5,26-35,42] Further TEM data that show the presence of 3 × 3 tunnels and dark field images for these materials will be presented elsewhere.[43] The conducting nature of the M-OMS-1 samples is consistent with the stability of these samples in the TEM experiments.

The tunnel structure of the OMS-1 samples is also supported by computer modeling studies. Simulated XRD patterns are basically the same as the corresponding observed patterns. The

(43) Wasserman, S. R.; Carrado, K. A.; Yuchs, S.; Shen, Y. F.; Cao, M.; Suib, S. L. *Physica B* **1994**, in press.

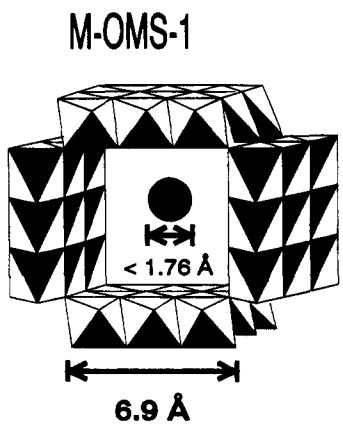

Figure 16. Model showing maximum cation diameter for inorganic cation templates for M-OMS-1 materials.

peaks at 9.6 and 4.8 Å have been indexed as the (100) and (020) planes of todorokite, respectively.[4-6]

As far as the coordination of the template cations is concerned, EPR results show an octahedral coordination of both Mn^{2+} (in all samples) and Cu^{2+} in Cu-OMS-1. EXAFS and XANES data for the Cu system are also consistent with octahedral Cu^{2+}.[43] For the other cations, octahedral coordination has not been confirmed, although indirect evidence exists. Zn^{2+} is found to be octahedrally coordinated in the interlayer of the layered mineral chalcophanite, $ZnMn_3O_7 \cdot 3H_2O$.[19] The fact that Zn-OMS-1 is not very stable and readily converts to a spinel phase suggests it is present at low temperature in an octahedral field and then converts to a tetrahedral geometry. $Co(H_2O)_6^{2+}$ and $Ni(H_2O)_6^{2+}$ are extremely stable in aqueous solution and are believed to serve as templates here. Mg^{2+} is also octahedrally coordinated in Mg_6MnO_8.[44] On the other hand, all five divalent cations studied here have similar sizes in 6-fold coordination (Table 1), which may yield similar tunnel sizes or interlayer distances in the tunnel or layered materials, respectively. Therefore, on the basis of diffraction, spectroscopy, and microscopy experiments, it is reasonable to conclude that Cu^{2+} and Mn^{2+} are octahedral in M-OMS-1 materials and it is likely that Mg^{2+}, Co^{2+}, Ni^{2+}, and Zn^{2+} cations are also octahedrally coordinated. A model showing the maximum cation diameter (solid sphere) for M-OMS-1 materials is given in Figure 16.

2. Composition, Manganese Oxidation States, and Thermal Stability. Unit cell formulas have been estimated from the above ICP, TGA, and titration results by assuming 12 oxygen atoms per unit cell. These formulas are as follows: $Mg_{3.17}Mn_{5.05}O_{12} \cdot 4.52H_2O$, $Co_{1.84}Mn_{5.59}O_{12} \cdot 3.45H_2O$, $Ni_{1.64}Mn_{5.75}O_{12} \cdot 4.19H_2O$, $Cu_{3.50}Mn_{4.45}O_{12} \cdot 5.33H_2O$, and $Zn_{3.55}Mn_{4.47}O_{12} \cdot 2.59H_2O$.

The formulas show that Co^{2+} and Ni^{2+} cations have significantly smaller contents than the other three cations (Table 3). This difference is not due to incomplete ion-exchange of Na^+ by Co^{2+} or Ni^{2+}, since XRD patterns show no peaks for Na^+-birnessite in Co^{2+}- and Ni^{2+}-buserite samples and SEM/EDX data do not show Na^+ on Co^{2+}- and Ni^{2+}-todorokite. It is not clear what causes such differences in cation content; however, similar observations have been observed for manganese nodules.[45]

No correlation is found between thermal stability and cation content. Therefore, the effect of cations on thermal stability may be related to the nature of such cations.

Thermal stability appears to be correlated with the average oxidation state of manganese (Table 3). The lower the average manganese oxidation state, the greater the thermal stability. On the basis of such a relationship between thermal stability and the manganese oxidation state, these OMS-1 materials can be divided into the following three groups: Mg-OMS-1 with the highest thermal stability (600 °C) and the lowest average manganese oxidation state (3.5), Cu- and Zn-OMS-1 with the least thermal stability (300 °C), and the highest manganese oxidation state (3.8), and Co- and Ni-OMS-1 which are in an intermediate region. Since all five OMS-1 samples were prepared from the same precursor (Na^+-birnessite), a lower average manganese valency is an indication of a loss of Mn^{2+} and probably Mn^{3+} during ion-exchange and/or autoclaving. The loss of Mn^{2+} and Mn^{3+} ions may be due to substitution or displacement of Mn^{2+} and Mn^{3+} by these other cations. Such substitution or displacement decreases in the order Zn = Cu > Co = Ni > Mg. Manganese contents of these OMS-1 samples (Table 3) appear to support this explanation.

A reviewer has suggested that the thermal and acidity properties are related. It is clear that the least thermally stable materials are the least acidic (Cu-OMS-1, Zn-OMS-1). However, for the more thermally stable materials (Mg, Co, Ni) there is no direct correlation with acidity. This may be related to metal content, site location, polarizability, and other factors.

Conclusions

Manganese oxide OMS-1 materials with different transition-metal cation templates have successfully been synthesized. The OMS-1 samples have a tunnel size of about 6.9 Å and different divalent cations in the tunnel as well as Mn^{2+} ions in an octahedral environment. They have pure chemical compositions and show good crystallinity. The template cations have significant effects on the physicochemical properties of the OMS-1 materials such as conductivity,[6,46] magnetic properties,[47] and catalytic oxidations.[4,5] Five hydrated cations, Mg^{2+}, Co^{2+}, Ni^{2+}, Cu^{2+}, and Zn^{2+}, have been successfully used to synthesize five OMS-1 materials with the todorokite structure and the following formulas: $Mg_{3.17}Mn_{5.05}O_{12} \cdot 4.52H2O$, $Co_{1.84}Mn_{5.59}O_{12} \cdot 3.45H_2O$, $Ni_{1.64}Mn_{5.75}O_{12} \cdot 4.19H_2O$, $Cu_{3.50}Mn_{4.45}O_{12} \cdot 5.33H_2O$, and $Zn_{3.55}Mn_{4.47}O_{12} \cdot 2.59H_2O$. The hydrated transition-metal cations serve as templates since lattice parameters determined from TEM are cation dependent. Thermal stability largely depends on the nature of the cations. Mg-OMS-1 can be stable in air up to 600 °C, Co-OMS-1 and Ni-OMS-1 are stable to 500 °C, and Cu-OMS-1 and Zn-OMS-1 are stable to 300 °C. All five OMS-1 samples can be calcined in air to corresponding spinel compounds, but require different temperatures to do so. Mg-OMS-1 is converted to $MgMn_2O_4$ at 700 °C, Co-OMS-1 and Ni-OMS-1 are converted to unknown crystalline compounds at 600 °C and corresponding spinel compounds at 700 °C, and Cu-OMS-1 and Zn-OMS-1 start to be converted to $CuMn_2O_4$ and $ZnMn_2O_4$ at 400 and 300 °C, respectively. Acidity is affected by the nature of template cations. Mg-OMS-1, Co-OMS-1, Zn-OMS-1, and Ni-OMS-1 have intermediate strength Brønsted and Lewis acid sites, while Cu-OMS-1 has no Brønsted acid sites and weak Lewis acid sites.

Acknowledgment. We thank the Department of Energy, Office of Basic Energy Sciences Division of Chemical Sciences, and Texaco, Inc. for support of this research. We thank Professors A. Clearfield, M. E. Davis, J. B. Dixon, and L. Kevan and Dr. L. E. Iton for helpful discussions.

(44) Porta, P.; Valigi, M. *J. Solid State Chem.* **1973**, *6*, 34-36.
(45) Baturin, G. N. *The Geochemistry of Manganese and Manganese Nodules in the Ocean*; D. Reidel Publishing Co.: Dordrecht, The Netherlands, 1988.
(46) (a) DeGuzman, R. N. M.S. Thesis, University of Connecticut, 1994. (b) DeGuzman, R. N.; Awaluddin, A.; Suib, S. L.; O'Young, C. L. *Chem. Mater.* submitted for publication.
(47) Suib, S. L.; Iton, L. E. *Chem. Mater.* **1994**, *6*, 429-433.